Nano Res (2010) 3: 379–386
DOI 10.1007/s12274-010-1042-0
Research Article

Bi_2S_3 Nanostructures: A New Photocatalyst

Tong Wu, Xinggui Zhou, Hua Zhang (✉), and Xinhua Zhong (✉)

State Key Laboratory of Chemical Engineering, Department of Chemistry, East China University of Science and Technology, Shanghai 200237, China

Received: 26 February 2010 / Revised: 28 March 2010 / Accepted: 30 March 2010

ABSTRACT

Uniform colloidal Bi_2S_3 nanodots and nanorods with different sizes have been prepared in a controllable manner via a hot injection method. X-ray diffraction (XRD) results show that the resulting nanocrystals have an orthorhombic structure. Both the diameter and length of the nanorods increase with increasing concentration of the precursors. All of the prepared Bi_2S_3 nanostructures show high efficiency in the photodegradation of rhodamine B, especially in the case of small sized nanodots—which is possibly due to their high surface area. The dynamics of the photocatalysis is also discussed.

KEYWORDS

Bi_2S_3, nanostructures, hot injection, photocatalyst

1. Introduction

Finding new ways of treating environmental pollution is great challenge and a major area of scientific study. As a result, many methods for the degradation of water contaminants have been developed. Photocatalytic degradation that uses visible or ultraviolet (UV) light as irradiating source is considered as a key method of water decontamination as it can bring fast and complete mineralization of pollutants without leaving any harmful residues and has recently become a vital technology [1–3]. Up to now, most photocatalysts have been based on metal oxides such as TiO_2 and ZnO. As a representative catalyst in the family, TiO_2 has shown excellent photocatalytic activity, especially when doped with C, N, B, or grown with a high percentage of specific crystal facets or heterojunction structures [4–9]. Besides metal oxides, some non-oxide compounds such as metal sulfides also show high efficiency in photodegradation. Theoretically, when any semiconductor with the appropriate band structure absorbs energy higher than its band gap under light irradiation, the resulting photo-generated electrons and holes will be separated by transfer to the particle surface or to another material and the system can serve as a catalyst for photocatalytic degradation. Compared to metal oxides such as TiO_2 and ZnO, metal sulfide photocatalysts may be more easy and convenient to fabricate via low cost using solution methods without the need to sacrifice crystallinity, monodispersity, and purity, since there is a greater choice of possible precursors for the preparation of metal sulfides. Furthermore, in the preparation of metal sulfides, the size and shape of the product can be conveniently tuned by varying the concentration of the precursor and/or the molar ratio of metal to sulfur precursors. In the last five years, the use of nanoscale metal sulfides as photocatalysts has attracted great

Address correspondence to Hua Zhang, zhanghjy@ecust.edu.cn; Xinhua Zhong, zhongxh@ecust.edu.cn

interest and several breakthroughs have been achieved. CuS, PbS, and CdS nanowires have been reported to have high efficiency in the degradation of rhodamine B and methyl orange under UV irradiation [10]. ZnS porous microspheres co-doped with N and C showed excellent photocatalytic activity in the degradation of Acid Orange 7 under visible light irradiation [11]. Sulfide–oxide composites such as Fe_3O_4/CdS nanocomposites also exhibit both excellent magnetic properties and high photocatalytic activity, even after 12 recycles, in the photodegradation of methyl orange in aqueous solution [12]. These limited reports indicate that, like oxides, nanoscale metal sulfide semiconductors also have photocatalytic activity and may be applied in environmental remediation.

Bismuth sulfide (Bi_2S_3) is a typical lamellar structured semiconductor with a bulk direct bandgap of 1.3 eV [13]. Nanostructures of this material have attracted much attention due to their potential applications such as in electrochemical hydrogen storage, hydrogen sensors, X-ray computed tomography imaging, biomolecule detection, and as photoresponsive materials [14–19]. However, the photocatalytic properties of Bi_2S_3 have been scarcely reported. In the only paper to date, SiO_2/Bi_2S_3 nanocomposites showed photocatalytic activity in the degradation of methylene blue, but SiO_2 alone in the absence of Bi_2S_3 also had degradation activity [20]. So, the photocatalytic activity of pure Bi_2S_3 is worth studying further from the viewpoints of both fundamental research and applications in environmental treatment. In recent years, Bi_2S_3 nanostructures with various morphologies—including nanotubes, nanorods or nanowires, nanoribbons, and nanocomposites—have been prepared via different methods [21–24]. Single crystal orthorhombic Bi_2S_3 nanostructures with various morphologies, including wires, rods, and flowers have been controllably prepared in a polyol solution process [25]. Hierarchical Bi_2S_3 core–shell structured microspheres have been fabricated by chemical transformation of BiOCl microspheres which also serve as a template [26]. It is well known that monodisperse nanoparticles with narrow size and shape distribution can be fabricated via the hot injection technique in high-boiling-point organic solvents [27, 28]. Bi_2S_3 nanostructures obtained by the organic solvent route have been reported by Ozin et al. [29, 30] and Li et al. [31].

Herein orthorhombic structured Bi_2S_3 nanodots and nanorods are controllably prepared via the hot injection technique by varying the experimental parameters including precursor concentrations and the molar ratio of Bi to S. Photocatalytic activities in the degradation of three typical dyes (methyl orange, methylene blue, and rhodamine B) are also studied and all of the prepared nanocrystals are found to have high photodegradation efficiency. The new photocatalysts have potential applications in environmental remediation.

2. Experimental

2.1 Chemicals

Oleylamine (OAm, 90%) was obtained from Acros. Bismuth(Ⅲ) chloride ($BiCl_3$, AR), thioacetamide (AR), methylene blue (MB, AR), rhodamine B (RhB, AR), methyl orange (MO, AR), and anhydrous ethanol (AR) were purchased from Sinoreagent. All chemicals were used as received without further purification. Double distilled water was used throughout the experiments.

2.2 Synthesis of Bi_2S_3 nanostructures

Bi_2S_3 nanostructures were synthesized by a reaction between bismuth chloride and thioacetamide using standard oxygen-free and hot injection techniques [27, 28]. Typically, 31.5 mg (0.1 mmol) of $BiCl_3$ powder was added to a flask containing 2.0 mL of OAm followed by degassing at 70 ℃ for 5 min under vacuum to remove the moisture and oxygen. The reaction vessel was then filled with nitrogen and the temperature was increased to 150 ℃ with a heating rate of 10 ℃/min and the vessel maintained at this temperature until the complete dissolution of $BiCl_3$ powder to give a white milky solution. Then 2.0 mL of OAm containing 11.3 mg (0.15 mmol) of thioacetamide was injected into the reaction system. After the addition of thioacetamide, the temperature of the reaction system was further increased to 180 ℃ and the vessel maintained at this temperature for 5–10 min. On introduction of thioacetamide, the color of the reaction mixture immediately changed from white to brown,

indicating the formation of Bi_2S_3. The growth of Bi_2S_3 nanostructures was terminated by removing the heating apparatus. The reaction mixture was cooled to room temperature and the resulting nanostructures were precipitated by anhydrous ethanol and washed several times and then dried in a vacuum oven at 60 ℃ for several hours to obtain the dry powder.

2.3 Characterization of structure and optical properties

The purity and structure of the products were confirmed by powder X-ray diffraction (XRD) obtained on a D8 Advance (Bruker) X-ray diffractometer equipped with graphite monochromatized high-intensity Cu Kα radiation (λ = 1.5406 Å) at 40 kV and 40 mA. XRD samples were prepared by depositing dry powder on a piece of glass. Transmission electron microscopy (TEM) measurements were performed on a JEOL-1400 transmission electron microscope with an acceleration voltage of 100 kV and high-resolution TEM (HRTEM) was performed on a JEOL-2010 high-resolution electron microscope with an acceleration voltage of 200 kV. The samples were prepared by dropping about 20 μL of a diluted solution of nanostructures in toluene onto carbon-coated copper grids and slowly drying in air. UV–visible absorption spectra were recorded on a Shimadzu UV-2450 spectrophotometer with a resolution of 1.0 nm. The *Brunauer*–Emmett–Teller (BET) surface areas of Bi_2S_3 powder were calculated from N_2 adsorption isotherms obtained using an ASAP 2010 instrument (Micromeritics, USA) at 77 K.

2.4 Photocatalytic tests

A 500-W mercury vapor lamp was used as the UV irradiation source. In a typical photocatalytic test, 10 mg of a nanostructured Bi_2S_3 powder was loaded in a quartz cell containing 40 mL of 20 mg/L dye (MO, MB, or RhB) solution. Prior to the start of the irradiation, dark adsorption was carried out for 1 h under continuous stirring to establish equilibrium between the dye and the catalyst. At a given time interval after commencement of irradiation, the dye concentration was monitored by measuring the maximum UV absorbance at 462, 663, and 553 nm for MO, MB, and RhB, respectively. The degradation efficiency (E%) was evaluated by the following formula,

$$E(\%) = (1 - C/C_o) \times 100\%$$

where C_o and C represent the absorbance of dye solution before and after irradiation, respectively.

3. Results and discussion

3.1 Structure and morphology

In our experiments, OAm was used as the ligand and also the solvent. The white homogeneous BiOCl obtained by transformation of $BiCl_3$ (a similar reaction was observed in Ref. [30]) reacted with the injected sulfur source at an intermediate temperature to form Bi_2S_3 rather than elemental bismuth due to the strong affinity between bismuth and sulfur. The lamellar structure of Bi_2S_3 results in anisotropic growth along the *c*-axis which favors the final formation of one-dimensional morphologies [32]. Figure 1 shows a typical XRD pattern of the resulting Bi_2S_3 nanocrystals. All the diffraction peaks can be indexed as the orthorhombic structured Bi_2S_3 with lattice constants of a = 11.14 Å, b = 11.30 Å, and c = 3.98 Å (JCPDS No. 17–0320) and the major peaks can be ascribed to 020, 120, 220, and 130 facets etc. The purity is confirmed by the absence of other peaks. Figures 2(a)–2(d) show typical TEM images of Bi_2S_3 nanocrystals prepared with different concentrations of precursor with a fixed Bi/S ratio of 1:1.5. All of the samples have a rod-like morphology. When the $BiCl_3$ precursor concentration was 0.025 mol/L, the nanorods (Fig. 2(a)) are uniform in size and shape with diameter of 7 nm ± 2 nm and lengths of 30–45 nm. On increasing the bismuth precursor concentration to 0.05 mol/L (Fig. 2(b)) and 0.1 mol/L (Fig. 2(c)), the diameters of the nanorods increased to 9 and 11 nm, respectively, and their lengths increased to 33–51 and 45–68 nm, respectively. When the concentration was further increased to 0.2 mol/L, the diameter of the resulting nanorods increased dramatically to 20 nm ± 4 nm and the length increased to 60–100 nm (Fig. 2(d)). It can be seen that the aspect ratio of the nanorods is almost independent of the precursor concentration. In contrast, in a previous preparation of Bi_2S_3 nanorods via the decomposition of bismuth di-*n*-octyl-dithiophosphates, when the

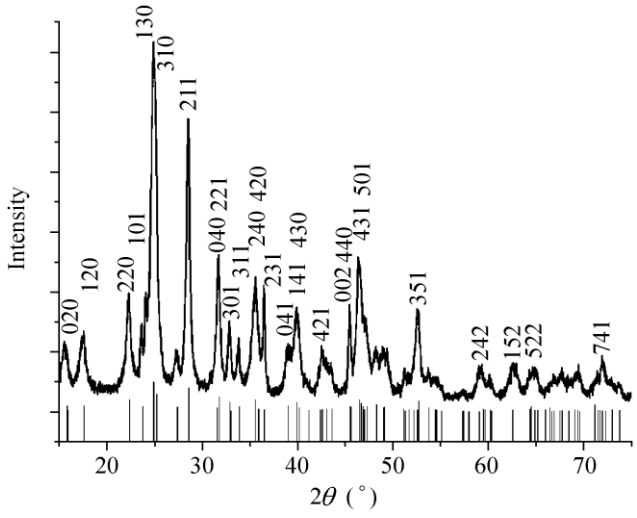

Figure 1 Typical XRD pattern of Bi_2S_3 nanostructures prepared with a Bi concentration of 0.025 mol/L and a Bi/S ratio of 1:1.5

precursor concentration was increased the diameter of the nanorods obtained did not change significantly, while the length decreased [33]. In the synthesis of nanomaterials via wet chemical routes, high precursor concentrations often accelarate nucleation or growth processes. In the synthesis of Bi_2S_3 nanorods in our system, the larger precursor concentrations may effectively speed up the growth rather than the nucleation, resulting in the larger diameters and lengths of the final nanorods. Figures 2(e) and 2(f) show HRTEM images of the nanorods with diameters of about 17 nm and 7 nm, respectively. In Fig. 2(e), the particle has continuous one-dimensional lattice fringes with a spacing of ~0.357 nm, corresponding to the (130) facet exhibiting the strongest peak in the XRD pattern. Although the fringes of the (001) facet are not observed in the image, it can still be supposed that the nanorods grow along the [001] direction, which is perpendicular to the (130) facet, as has been observed in previous reports [32]. In Fig. 2(f), the small nanorods have discontinuous and faint lattice fringes indicative of poor crystallinity, possibly due to either insufficient growth or electron beam irradiation [34].

The size of the Bi_2S_3 particles can be tuned by varying both the concentration of the precursor and the molar ratio of Bi to S. Figure 3 shows typical TEM images of Bi_2S_3 nanostructures prepared with different molar ratios of Bi to S for a fixed Bi precursor concentration of 0.025 mol/L. When the stoichiometric ratio (Bi:S = 1:1.5) was employed (Fig. 3(c)), the nanorods

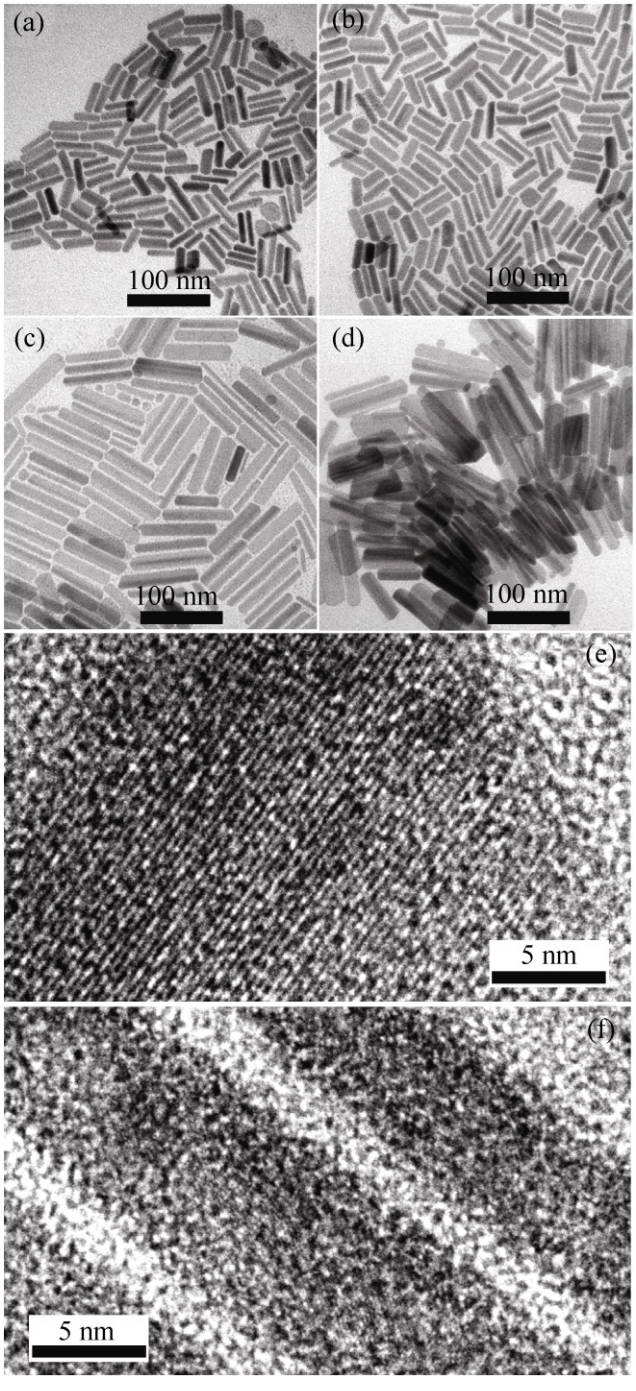

Figure 2 TEM image of Bi_2S_3 nanocrystals prepared with a Bi/S ratio of 1:1.5 and Bi precursor concentrations of (a) 0.025 mol/L, (b) 0.05 mol/L, (c) 0.1 mol/L, and (d) 0.2 mol/L. HRTEM images of typical Bi_2S_3 nanorods with diameters of (e) ~17 nm (from the sample in (d)) and (f) ~7 nm (from the sample in (a))

have diameter of 7 nm ± 2 nm and lengths of 30–45 nm (the same sample as shown in Fig. 2(a)). In the case of a deficiency of S (a molar ratio of Bi to S of 1:1, Fig. 3(b)), the nanorods have diameter of 8.5 nm ± 1 nm

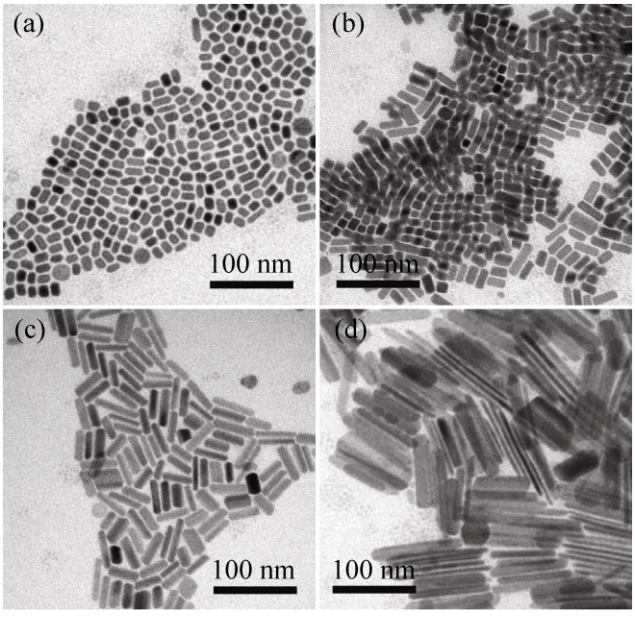

Figure 3 TEM images of Bi_2S_3 nanocrystals prepared with a Bi precursor concentration of 0.025 mol/L with Bi/S molar ratios of (a) 1:0.5, (b) 1:1, (c) 1:1.5, and (d) 1:1.7

with lengths of 9–20 nm. With a further decrease of S giving a Bi/S ratio of 1:0.5, the resulting Bi_2S_3 nanostructures have an elonged dot-like shape with diameter of 8 nm ± 0.5 nm and length of 12 nm ± 0.5 nm (Fig. 3(a)). When S is in excess (a Bi/S ratio of 1:1.7), a mixture of two types of nanorods with diameters of 4.5 nm or 17 nm, but with similar lengths of 104 nm ± 5 nm were obtained (Fig. 3(d)). From these results, it can be concluded that an excess of Bi leads to a reduction in the length of the nanorods and nearly no change in diameter, resulting in a small aspect ratio. When the amount of S is increased, the lengths of the resulting nanostructures are dramatically increased and the diameters become non-uniform for materials prepared under S-rich conditions. Thus, the size and shape of the Bi_2S_3 nanostructures can be conveniently controlled simply by tuning the concentrations and molar ratio in the precursor mixture.

3.2 Optical properties and photocatalytic activity

Figure 4 shows a typical UV–visible absorption spectrum of the Bi_2S_3 nanorods prepared with a Bi precursor concentration of 0.025 mol/L, Bi:S = 2:3. There are no absorption peaks in the spectrum, but a sharp absorption begins at about 400 nm. Figure 5 shows the efficiency of Bi_2S_3 nanorods (prepared with a Bi source concentration of 0.025 mol/L, Bi:S = 2:3) in the photodegradation of MB, MO, and RhB. In the case of RhB, the dye was decolorized completely after about 2 h (a degradation efficiency of ~100%). For MB only ~40% degradation efficiency could be obtained in the same period, and less than 70% of the dye was degraded even after 4 h in the case of MO. That is to say, Bi_2S_3 nanorods show higher photocatalytic activity for degradation of RhB than for MO or MB. So, we chose RhB for a detailed study of the dependence of the photocatalytic activity of Bi_2S_3 on its particle size. Figure 6(a) shows the degradation efficiency of Bi_2S_3 nanodots (the sample in Fig. 3(a)) and nanorods having different diameters but similar aspect ratio prepared with various Bi concentrations. In the case of the nanodots and thin nanorods (7 nm in diameter), the dye was nearly completely degraded after irradiation for 90 min, while in the case of larger nanorods corresponding to diameters of 9–20 nm, longer irradiation time (~200 min) is required to completely degrade the dye. From these results, it can be concluded that the degradation efficiency increases with decreasing diameter of the Bi_2S_3 nanodots and nanorods. This is possibly because the nanodots and small sized nanorods have larger surface areas than the larger nanorods. The BET specific surface areas of the samples in Fig. 6 arranged in order of decreasing degradation efficiency are 9.9, 8.1, 7.5, 6.7, and 5.2 m^2/g, respectively, which gives support to our conclusion.

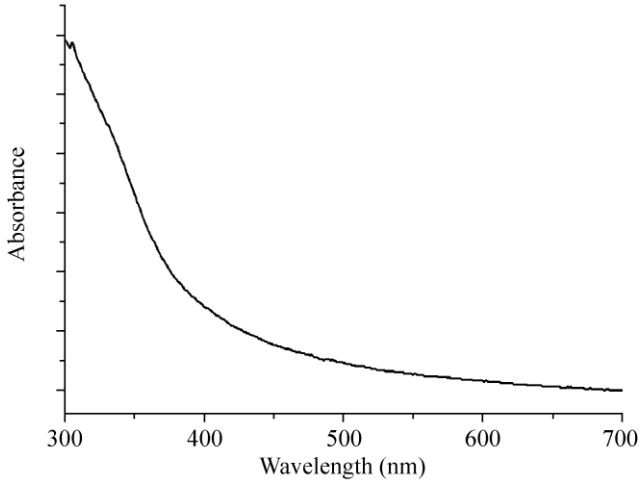

Figure 4 UV–visible absorption spectrum of Bi_2S_3 nanocrystals prepared with a Bi precursor concentration of 0.025 mol/L, Bi:S = 2:3

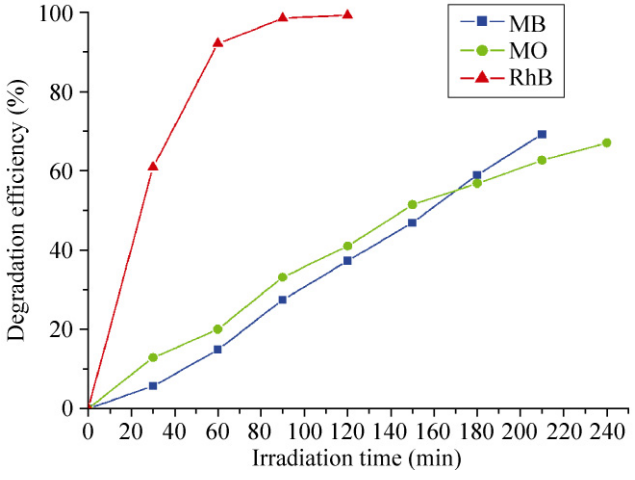

Figure 5 Photodegradation efficiency of Bi_2S_3 nanorods (prepared with a Bi source concentration of 0.025 mol/L, Bi:S = 2:3) with MO, MB, and RhB

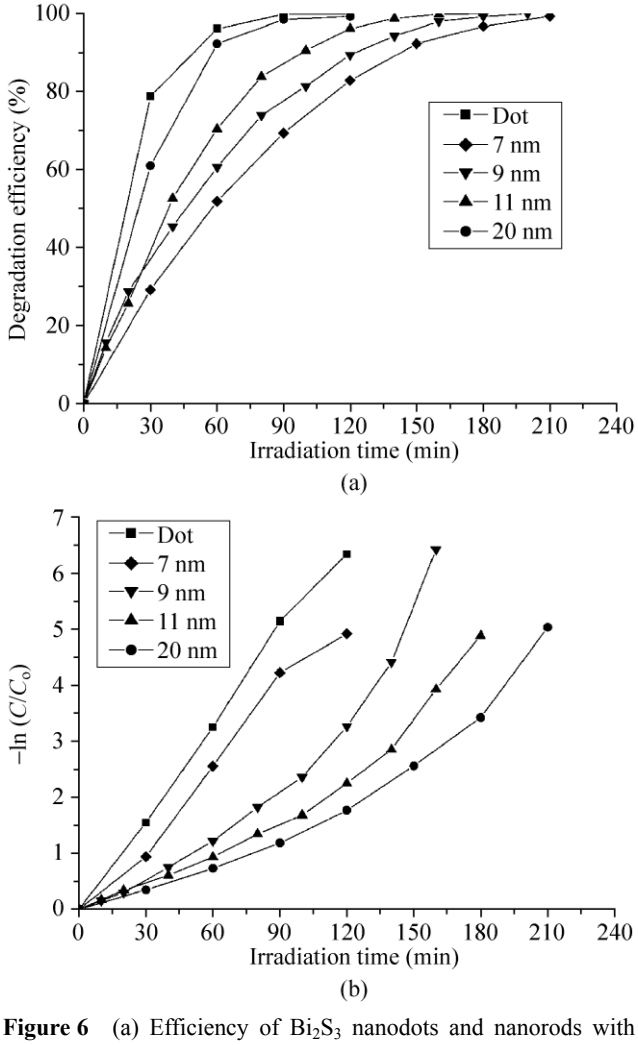

Figure 6 (a) Efficiency of Bi_2S_3 nanodots and nanorods with different diameters on the photodegradation of RhB and (b) the corresponding plots of $-\ln\frac{C}{C_o}$ vs. t (irradiation time)

To further investigate the mechanism, we studied the photocatalytic reaction dynamics. It has been well established that heterogeneous photocatalysis by semiconductors follows the Langmuir–Hinshelwood (LH) dynamic model [35],

$$\frac{1}{R}=\frac{1}{kK}\times\frac{1}{C_o}+\frac{1}{k}$$

where R is the reaction rate, k is the reaction rate constant, K is the adsorption equilibrium constant, and C_o is the initial dye concentration. When C_o is small, the reaction follows first order kinetics with a rate equation in the form

$$-\ln\frac{C}{C_o}=kKt=k't$$

where C is the dye concentration at time t, and k' is the apparent first order rate constant. Figure 6(b) shows plots of $-\ln\frac{C}{C_o}$ vs. t for Bi_2S_3 nanostructures with different particle sizes. In the plots for the nanodots with small diameter and aspect ratio, a good linearity was observed, indicative of first order kinetics. For each of the nanorod samples, the non-linear nature of the plots is inconsistent with first order kinetics. The deviation from linearity of the plots for the nanorods may result from their broad size distribution and anisotropic morphology. The slopes of the plots also show that the nanodots have higher photocatalytic activity than all of the nanorods. The influence of size and morphology of Bi_2S_3 nanostructures on the photodegradation kinetics should be further studied.

4. Conclusions

Orthorhombic Bi_2S_3 nanostructures have been prepared by the reaction between bismuth chloride and thioacetamide in oleylamine and the size and morphology of the resulting nanostructures can easily be tuned by varying the precursor concentrations and molar ratio of Bi to S. An excess of Bi favors the formation of nanostructures with small aspect ratio and narrow size distribution, while an excess of S favors the formation of nanorods. When a stoichiometric

mixture of precursors was employed, both the diameter and length of the nanorods increased with increasing concentration of bismuth precursor. All of the nanodots and nanorods have good photocatalytic activity for degradation of MO, MB, and RhB. The small nanodots have the highest degradation efficiency due to them having the largest surface area. Photocatalysis by nanodots may follow first order kinetics according to the LH model. Many aspects need to be further investigated, but the high photocatalytic activities suggest that the reported nanoscale Bi_2S_3 nanostructures have potential applications in the photocatalytic degradation of organic pollutants.

Acknowledgements

This work was financially supported by the National Natural Science Foundation of China (Nos. 20771037 and 20871047), the Shuguang Project (No. 06SG33), SRFDP (No. 20070251014), the State Key Laboratory of Chemical Engineering (No. SKL-ChE-09C01) and the Program for Professors by Special Appointment at Shanghai Institutions of Higher Learning.

References

[1] Prevot, A. B.; Basso, A.; Baiocchi, C.; Pazzi, M.; Marcí, G.; Augugliaro, V.; Palmisano, L.; Pramauro, E. Analytical control of photocatalytic treatments: Degradation of a sulfonated azo dye. *Anal. Bioanal. Chem.* **2004**, *378*, 214–220.

[2] Ameta, S. C.; Chaudhary, R.; Ameta, R.; Vardia, J. Photocatalysis: A promising technology for wastewater treatment. *J. Indian Chem. Soc.* **2003**, *80*, 257–265.

[3] Friesen, D. A.; Headley, J. V.; Langford, C. H. The photooxidative degradation of *N*-methylpyrrolidinone in the presence of $Cs_3PW_{12}O_{40}$ and TiO_2 colloid photocatalysts. *Environ. Sci. Technol.* **1999**, *33*, 3193–3198.

[4] Yang, H. G.; Liu, G.; Qiao, S. Z.; Sun, C. H.; Jin, Y. G.; Smith, S. C.; Zou, J.; Cheng, H. M.; Lu, G. Q. Solvothermal synthesis and photoreactivity of anatase TiO_2 nanosheets with dominant {001} facets. *J. Am. Chem. Soc.* **2009**, *131*, 4078–4084.

[5] Liu, G.; Yang, H. G.;Wang, X. W.; Cheng, L. N.; Pan, J.; Lu, G. Q.; Cheng, H. M. Visible light responsive nitrogen doped anatase TiO_2 sheets with dominant {001} facets derived from TiN. *J. Am. Chem. Soc.* **2009**, *131*, 12868–12869.

[6] Bian, Z. F.; Zhu, J.; Wang, S. H.; Cao, Y.; Qian, X. F.; Li, H. X. Self-assembly of active Bi_2O_3/TiO_2 visible photocatalyst with ordered mesoporous structure and highly crystallized anatase. *J. Phys. Chem. C* **2008**, *112*, 6258–6262.

[7] Zaleska, A.; Sobczak, J. W.; Grabowska, E.; Hupka, J. Preparation and photocatalytic activity of boron-modified TiO_2 under UV and visible light. *Appl. Catal. B* **2008**, *78*, 92–100.

[8] Bessekhouad, Y.; Robert, D.; Weber, J. V. Photocatalytic activity of Cu_2O/TiO_2, Bi_2O_3/TiO_2, and $ZnMn_2O_4/TiO_2$ heterojunctions. *Catal. Today* **2005**, *101*, 315–321.

[9] Gombac, V.; Rogatis, L. D.; Gasparotto, A.; Vicario, G.; Montini, T.; Barreca, D.; Balducci, G.; Fornasiero, P.; Tondello, E.; Graziani, M. TiO_2 nanopowders doped with boron and nitrogen for photocatalytic applications. *Chem. Phys.* **2007**, *339*, 111–123.

[10] Zhang, F.; Wong, S. S. Controlled synthesis of semiconducting metal sulfide nanowires. *Chem. Mater.* **2009**, *21*, 4541–4554.

[11] Muruganandham, M.; Kusumoto, Y. Synthesis of N, C codoped hierarchical porous microsphere ZnS as a visible light-responsive photocatalyst. *J. Phys. Chem. C* **2009**, *113*, 16144–16150.

[12] Liu, X. W.; Fang, Z.; Zhang, X. J.; Zhang, W.; Wei, X. W.; Geng, B. Y. Preparation and characterization of Fe_3O_4/CdS nanocomposites and their use as recyclable photocatalysts. *Cryst. Growth Des.* **2009**, *9*, 197–202.

[13] Vogel, R.; Hoyer, P.; Weller, H. Quantum-sized PbS, CdS, Ag_2S, Sb_2S_3, and Bi_2S_3 particles as sensitizers for various nanoporous wide-bandgap semiconductors. *J. Phys. Chem.* **1994**, *98*, 3183–3188.

[14] Bao, H.; Li, C. M.; Cui, X. Q.; Gan, Y.; Song, Q. L.; Guo, J. Synthesis of a highly ordered single-crystalline Bi_2S_3 nanowire array and its metal/semiconductor/metal back-to-back Schottky diode. *Small* **2008**, *4*, 1125–1129.

[15] Rabin, O.; Perez, J. M.; Grimm, J.; Wojtkiewicz, G.; Weissleder, R. An X-ray computed tomography imaging agent based on long-circulating bismuth sulphide nanoparticles. *Nat. Mater.* **2006**, *5*, 118–122.

[16] Cademartiri, L.; Scotognella, F.; O'Brien, P. G.; Lotsch, B. V.; Thomson, J.; Petrov, S.; Kherani, N. P.; Ozin, G. A. Cross-linking Bi_2S_3 ultrathin nanowires: A platform for nanostructure formation and biomolecule detection. *Nano Lett.* **2009**, *9*, 1482–1486.

[17] Yao, K.; Gong, W. W.; Hu, Y. F.; Liang, X. L.; Chen, Q.; Peng, L. M. Individual Bi_2S_3 nanowire-based room-temperature H_2 sensor. *J. Phys. Chem. C* **2008**, *112*, 8721–8724.

[18] Li, L. S.; Sun, N. J.; Huang, Y. Y.; Qin, Y.; Zhao, N. N.; Gao, J. J.; Li, M. H.; Zhou, H. H.; Qi, L. M. Topotactic transformation of single-crystalline precursor discs into disc-like Bi_2S_3 nanorod networks. *Adv. Funct. Mater.* **2008**, *18*, 1194–1201.

[19] Bao, H. F.; Li, C. M.; Cui, X. Q.; Song, Q. L.; Yang, H. B.; Guo, J. Single-crystalline Bi_2S_3 nanowire network film and its optical switches. *Nanotechnology* **2008**, *19*, 335302.

[20] Albuquerque, R.; Neves, M. C.; Mendonca, M. H.; Trindade, T.; Monteiro, O. C. Adsorption and catalytic properties of SiO_2/Bi_2S_3 nanocomposites on the methylene blue photo-decolorization process. *Colloids Surf. A* **2008**, *328*, 107–113.

[21] Stavila, V.; Whitmire, K. H.; Rusakova, I. Synthesis of Bi_2S_3 nanostructures from bismuth(III) thiourea and thiosemicarbazide complexes. *Chem. Mater.* **2009**, *21*, 5456–5465.

[22] Wang, D. S.; Hao, C. H.; Zheng, W.; Ma, X. L.; Chu, D. R.; Peng, Q.; Li, Y. D. Bi_2S_3 nanotubes: Facile synthesis and growth mechanism. *Nano Res.* **2009**, *2*, 130–134.

[23] Fan, D. B.; Thomas, P. J.; O'Brien, P. Synthesis and assembly of Bi_2S_3 nanoparticles at the water–toluene interface. *Chem. Phys. Lett.* **2008**, *465*, 110–114.

[24] Ye, C. H.; Meng, G. W.; Jiang, Z.; Wang, Y. H.; Wang, G. Z.; Zhang, L. D. Rational growth of Bi_2S_3 nanotubes from quasi-two-dimensional precursors. *J. Am. Chem. Soc.* **2002**, *124*, 15180–15181.

[25] Quan, Z.; Yang, J.; Yang, P. P.; Wang, Z. L.; Li, C. X.; Lin, J. Facile synthesis and characterization of single crystalline Bi_2S_3 with various morphologies. *Cryst. Growth Des.* **2008**, *8*, 200–207.

[26] Li, L. S.; Cao, R. G.; Wang, Z. J.; Li, J. J.; Qi, L. M. Template synthesis of hierarchical Bi_2E_3 (E = S, Se, Te) core–shell microspheres and their electrochemical and photoresponsive properties. *J. Phys. Chem. C* **2009,** *113,* 18075–18081.

[27] Zhang, Y. L.; Zhu, J.; Song, X.; Zhong, X. H. Controlling the synthesis of CoO nanocrystals with various morphologies. *J. Phys. Chem. C* **2008**, *112*, 5322–5327.

[28] Zhong, X. H.; Feng, Y. Y.; Zhang, Y. L.; Lieberwirth, I.; Knoll, W. Nonhydrolytic alcoholysis route to morphology-controlled ZnO nanocrystals. *Small* **2007**, *3*, 1194–1199.

[29] Cademartiri, L.; Malakooti, R.; Brien, P. G. O.; Migliori, A.; Petrov, S.; Kherani, N. P.; Ozin, G. A. Large-scale synthesis of ultrathin Bi_2S_3 necklace nanowires. *Angew. Chem. Int. Ed.* **2008**, *47*, 3814–3817.

[30] Malakooti, R.; Cademartiri, L.; Akçakir, Y.; Petrov, S.; Migliori, A.; Ozin, G. A. Shape-controlled Bi_2S_3 nanocrystals and their plasma polymerization into flexible films. *Adv. Mater.* **2006**, *18*, 2189–2194.

[31] Wang, D. S.; Zheng, W.; Hao, C. H.; Peng, Q.; Li, Y. D. A synthetic method for transition-metal chalcogenide nanocrystals. *Chem. Eur. J.* **2009**, *15*, 1870–1875.

[32] Wang, Y.; Chen, J.; Wang, P.; Chen, L.; Chen, Y. B.; Wu, L. M. Syntheses, growth mechanism, and optical properties of [001] growing Bi_2S_3 nanorods. *J. Phys. Chem. C* **2009**, *113,* 16009–16014.

[33] Lou, W. J.; Chen, M.; Wang, X. B.; Liu, W. M. Novel single-source precursors approach to prepare highly uniform Bi_2S_3 and Sb_2S_3 nanorods via a solvothermal treatment. *Chem. Mater.* **2007**, *19,* 872–878.

[34] Kim, D.; Shimpi, P.; Gao, P. X. Zigzag zinc blende ZnS nanowires: Large scale synthesis and their structure evolution induced by electron irradiation. *Nano Res.* **2009**, *2*, 966–974.

[35] Tsunoyama, H.; Ichikuni, N.; Tsukuda, T. Microfluidic synthesis and catalytic application of PVP-stabilized, ~1 nm gold clusters. *Langmuir* **2008**, *24*, 11327–11330.